energies

MDPI

Article

Wave-Turbulence Decomposition Methods Applied to Tidal Energy Site Assessment

Larissa Perez [1,*], Remo Cossu [1], Camille Couzi [2] and Irene Penesis [2]

[1] School of Civil Engineering, University of Queensland, Brisbane 4072, QLD, Australia; r.cossu@uq.edu.au
[2] Australian Maritime College, University of Tasmania, Hobart 7250, TAS, Australia; camille.couzi@utas.edu.au (C.C.); i.penesis@utas.edu.au (I.P.)
* Correspondence: l.perez@uqconnect.edu.au

Received: 7 February 2020; Accepted: 5 March 2020; Published: 7 March 2020

Abstract: High levels of turbulence have been proven to substantially increase the blade loadings on tidal turbines, outlining the need of properly characterizing turbulence parameters in tidal energy sites. The presence of long surface gravity waves may cause a significant bias on the estimation of these parameters, which requires wave-turbulence decomposition methods that are currently missing from guidelines. Here, three techniques of decomposing wave and turbulence are tested: the stopband filter (SB), moving average filter (MA), and synchrosqueezing wavelet transform (SWT). The study site, Banks Strait, Tasmania, is a 16 km wide channel that presents high potential for tidal energy generation. Wave peak periods at the study site were found to vary mostly between 7 and 12 s, with maximum exceeding 15 s. Turbulence intensities (TI), turbulent kinetic energy (TKE), and integral scales are quantified. Our results indicate differences between the estimates obtained from each method. The MA highly underestimates turbulence, resulting in TI values which were nearly 50% lower than those obtained from other decomposition methods. While TI and TKE estimated from the SB and the SWT techniques are quite similar, integral length scales are considerably underestimated by the SB. These findings reveal that the SWT is a more reliable method because of the more accurate estimates of turbulence parameters and indicate the need of establishing guidelines which address wave-turbulence decomposition in tidal stream energy site assessments. Despite having shown to be quite a versatile technique, further investigation of its applicability in data from other prospective tidal energy sites is necessary to fully assess the generality of the SWT technique.

Keywords: tidal energy; site assessment; wave-current interaction; turbulence; integral length scales; wave-turbulence decomposition

1. Introduction

The ocean stores a vast amount of energy that can be harvested, for instance, from tidal currents. Prospective tidal energy sites are potentially highly energetic locations commonly characterized by high levels of turbulence and large waves, which can considerably increase loads on structures [1,2]. Hence, the research effort has been directed toward advancing tidal stream technologies to ensure they are reliable yet cost-effective. For instance, significant loads on a tidal turbine are caused by thrust forces, which tend to cause flapwise bending moments, and inertial forces, which cause chordwise bending moments. This implies that the rotor experiences extremely high dynamic forces because of the passing waves, turbulence, vortex shedding, and velocity shear, resulting in high bending moments [3]. These forces can lead to fatigue of the blade and hence are an important aspect to be considered when designing these devices. As highlighted by Ouro et al. [4] and Vazquez et al. [5], tidal energy LCOE still represents a challenge for it to become a mature technology, being highly related to the turbine's manufacturing and maintenance costs. Nonetheless, turbine developers have been overly conservative

because of an uncertainty regarding extreme loads, which significantly increases the levelized cost of energy (LCOE) [6]. Despite having an effect on blade loadings, the presence of fine-scale velocity fluctuations does not increase resource uncertainty substantially, reinforcing the predictability of this source of energy [7].

Laboratory experiments conducted by Blackmore et al. [8] showed that variations in turbulence intensity and length scales affect the turbine power and thrust coefficients by over 10%, highlighting the significance of turbulence to turbine performance. The results obtained from the laboratory work reported by Mycek et al. [9] revealed turbulence intensities did not affect the mean power and thrust coefficients substantially but it increased the standard deviations, which may lead to device fatigue. On a full-scale turbine, Harrold and Ouro [2] investigated the loadings on a 12 m diameter tidal turbine deployed in Ramsey Sound, UK. Observation of low and high frequency variations at turbine loadings indicated the presence of a variety of length scales and led to the conclusion that quantifying turbulence parameters is important to guarantee the device's long-term functionality. These results highlight the need to obtain accurate site-specific estimates of turbulence characteristics to ensure the optimum performance of tidal turbines and avoid unnecessary conservativeness and premature fatigue [10–14].

The presence of long surface gravity waves may result in orbital velocities reaching deeper parts of the water column. As a consequence, velocity fluctuations are no longer governed strictly by turbulence, but also by wave orbital motion, and turbulence parameters may be considerably overestimated [15–18]. In order to ensure more accurate estimates of turbulence parameters, and thus avoiding excessive levels of conservativeness, wave orbital motion and turbulent fluctuations must be decomposed in the total velocity fluctuation. Although the literature presents a variety of methods to perform wave-turbulence decomposition, little has been discussed regarding the practicality and applicability of these methods for characterization of turbulence in a tidal energy site assessment. For instance, the work by Parkinson and Collier [19] using the software Tidal Bladed (DNV GL, Bristol, UK), well-known in the industry, validated the results using acoustic Doppler current profiler (ADCP) data from the Fall of Warness. When addressing wave-turbulence interaction, the authors excluded periods of high wave activity in the analysis. The lack of best practice is further emphasized by the fact that the International Electrotechnical Commission (IEC) guidelines as well as, the European Marine Energy Centre (EMEC) do not include recommendations regarding criteria for turbulence measurements, wave-turbulence interaction, and wave-turbulence decomposition. To the authors' knowledge, the present work is the first to test and compare the wave-turbulence decomposition methods for a tidal energy site characterization and to report high frequency measurements taken over such a long period.

Since turbulent and wave orbital motion are usually overlapped on the same frequency bands, it can be argued that performing this task is not as trivial as band-pass filtering [20,21]. Nonetheless, this approach has still been adopted by several researchers [15,18,22,23]. Alternatively, Soulsby and Humphrey [24] have developed a technique based on separating wave induced motion and turbulent fluctuations within the frequency domain. It is assumed that the area under the energy spectrum is equal to the total velocity variance. By extrapolating the expected inertial subrange −5/3 slope [25], orbital velocity variance can be subtracted from the total variance. This technique, however, relies on the assumption that the energy peak caused by waves happens in the isotropic inertial subrange, which is not always the case. Another method is based on the phase lag between horizontal and vertical velocities at the wave frequencies [20]. However, since this method addresses directly the horizontal and vertical velocities, rather than beam velocities, it is not the most appropriate choice for data collected with ADCPs, as turbulence estimates from these instruments rely on the variance method [26,27]. This decomposition has also been successfully performed with a moving average filter, under the assumption that the filter result is the parcel of fluctuations attributed to waves [18,28]. Smyth et al. [15] have described and compared three methods of decomposing wave and turbulence. The first one was the filter method—applying a band-pass filter to the signal. The second one was based on the estimation of vertical wave velocity by assuming linear wave theory. Lastly, a technique

based on turbulence dissipation rate was applied. Resulting profiles of vertical root-mean-square velocities have shown to be very similar for the three methods and that the filter and the linear wave theory methods produce reasonable estimates of the turbulence intensity profiles. Similarly, Bian et al. [21] tested and compared three existing decomposition methods—the coherence, cospectra, and ensemble empirical mode decomposition (EEMD)—as well as introduced the synchrosqueezing wavelet transform (SWT), a signal processing technique based on wavelet transforms combined with the reallocation method [29]. Tests were conducted with acoustic Doppler velocimeter (ADV) data for estimation of Reynolds stresses. Even though all four methods slightly underestimated turbulence, the SWT method performed best.

In this paper we compare three techniques to conduct wave-turbulence decomposition for estimation of turbulence parameters at tidal energy sites: the stopband (SB) method, the moving average (MA) method, and the SWT method. While the first two are well-known filtering techniques, the latter is a novel signal processing method promising to provide accurate frequency estimates. These methods were chosen for comparison based on their different levels of practicality, sophistication, and computational time. The SB and MA are relatively simple, hence easily reproducible, and require little computational resources. Moreover, the debate in the literature regarding the applicability of the SB to wave-turbulence decomposition is still ongoing. Contrastingly, the SWT is a more complex and computationally demanding technique, which has provided more accurate results when compared to other methods [20]. The study site—Banks Strait, Tasmania—has been investigated for the Australian Tidal Energy (AUSTEn) project [30–32]. Analyzed data were collected by two Nortek Signature AD2CPs, deployed between March and July 2018, and a Nortek acoustic wave and current profiler (AWAC), deployed between March and May 2018. Instruments were configured to measure wave parameters, current velocities, and high-frequency velocity variations. A link to the dataset used for this work is available in the Supplementary Materials section. A wave climate and current characterization is conducted initially, followed by the application of the three decomposition methods and the estimation of turbulence intensities, turbulent kinetic energy, and integral scales. Finally, estimates obtained from each method are compared. The findings of this work provide important information to allow for the elaboration of guidelines for wave-turbulence decomposition and turbulence characterization in prospective tidal energy sites.

2. Materials and Methods

2.1. Study Site and Data Collection

Banks Strait is a promising site for tidal stream energy generation in Australia. It is a 15-km wide tidal channel located in the Eastern part of Bass Strait, Northeast Tasmania, between Swan and Clarke Islands. The depth in the area varies mostly between 25 and 60 m, with some deeper areas reaching over 70 m, and it has been highlighted for being suitable for tidal energy converters [30] (Figure 1). Even though this area does not exhibit large tidal ranges, strong tidal currents are prevalent. Power density has been estimated to be higher in the middle to northern side of the channel, reaching over 2000 W/m^2 and presenting stronger currents during ebb tides [31,33]. The dominant tidal harmonics constituents are M2 and N2, which are the principal and large elliptical lunar semidiurnal constituents respectively. Maximum current speeds at the site were found to reach over 2 m/s, with significant variation across the channel. Significant wave heights vary mostly between 1 and 2 m, with maximum values reaching over 5 m. Wave periods in Banks Strait vary dominantly between 7 and 12 s. Because of its geomorphology and dominant wind and current directions, the area is subject to strong wave-current interaction, requiring wave-turbulence decomposition prior to estimation of turbulence parameters [32].

During the deployment period dominant wind direction was West-Northwest. Maximum wind speeds have reached over 60 km/h, with approximately 80% of values below 35 km/h and mean speeds of approximately 20 km/h [34].

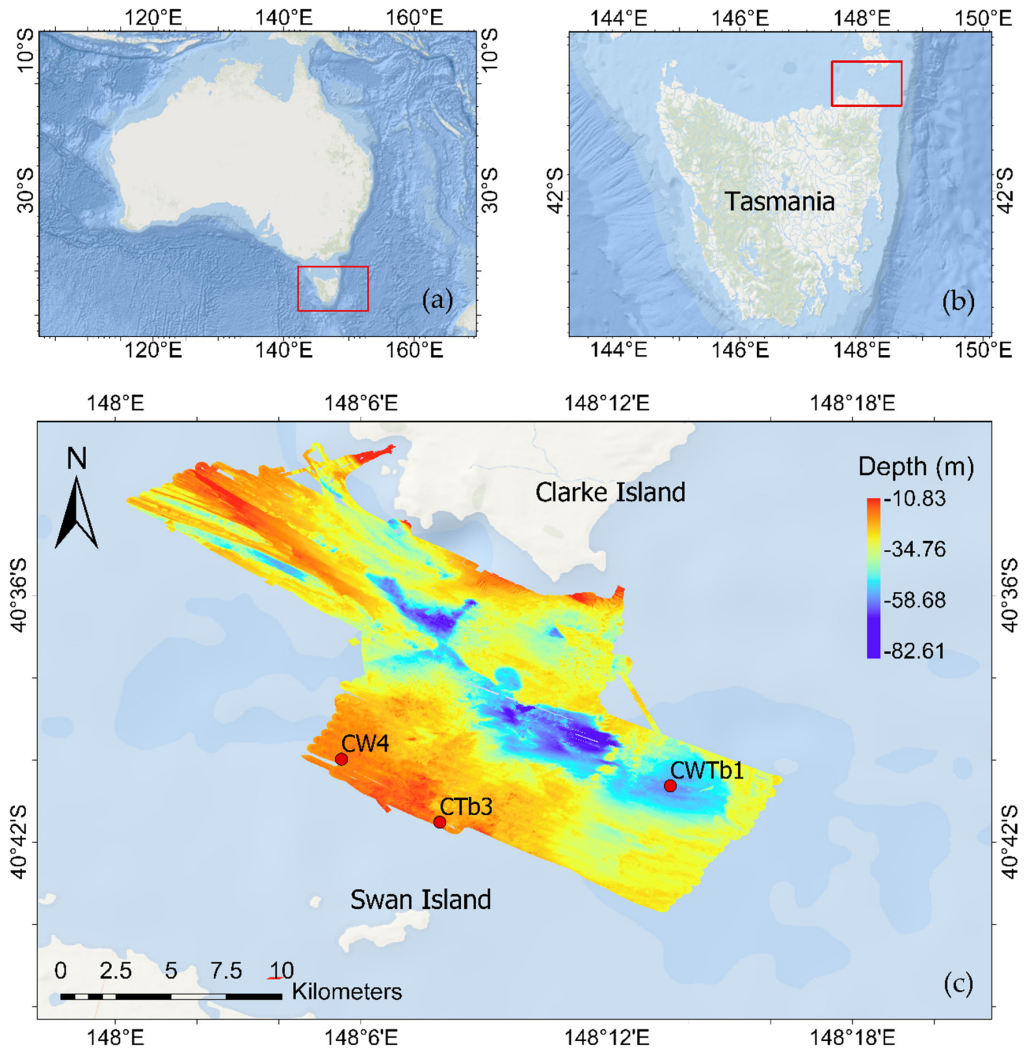

Figure 1. Indication of (**a**) Tasmania in Australia, (**b**) Banks Strait, Northeast Tasmania, and (**c**) measurement sites, located between Clarke and Swan Islands. (Sources: Esri, Garmin, GEBCO, NOAA NGDC and other contributors).

This work analyses data collected with two Nortek AD2CP Signature instruments (500 kHz and 1000 kHz) and a Nortek AWAC 1000 kHz. Investigated depths for turbulence estimation consider as reference a hub-height of 15 m above seabed. Bottom tip and top tip are defined as 10 and 20 m above seabed respectively. Figure 1 shows the deployment location for all three instruments. The signature series is a new generation ADCP that includes a fifth vertical beam. The instrument has a high sampling frequency (up to reach 16Hz depending of chosen configurations) as well as the ability to interleave between two acoustic measurement configurations during a single deployment. Thus, the signature instruments can obtain current velocity, turbulence, and wave data during the same deployment [35].

The Nortek Signature 1000 kHz (CTb3) was deployed in the southern side of the channel (40.5454° S, 148.078° E) at a depth of 33 m, between March and July 2018. In order to ensure data quality, samples which presented low amplitude or high amplitude spikes were removed as well as the top 10% of the water column, to avoid side lobe interference. As per manufacturer's recommendations, samples with beam correlation below 50% were also discarded.

The Nortek Signature 500 kHz (CWTb1) was deployed in the center of the channel (40.6772° S, 148.226° E), in approximately 60 m between March and July 2018. This instrument was set to interleave two different configuration plans. In the first configuration plan, CWTb1 was set to measure the current velocities and turbulence. In the second configuration plan, the instrument was set to measure the

current velocities and waves. Configuration for current measurements was the same for the first and second plan. For estimation of directional wave parameters, the instrument measures velocity with its four slanted beams, while using its vertical beam for acoustic surface tracking (AST). Data processing for quality control was done similarly to instrument CTb3.

A Nortek AWAC 1000 kHz (CW4) was set to measure current velocities and waves. The instrument was placed close to CTb3 (40.6664° S, 148.092° E), at a depth of 30 m, and was measuring between March and May 2018. Top of water column was removed in order to avoid side-lobe interference. All instruments were mounted on gravity-based moorings 1 m above the seafloor. Data were corrected for magnetic declination. Instruments configurations are summarized in Table 1.

Table 1. Summary of instruments configurations and deployment details.

Station	**CTb3**	**CWTb1**	**CW4**
Instrument	Signature 1000 kHz	Signature 500 kHz	AWAC 1000 kHz
Depth	33 m	60 m	30 m
Latitude	40.5454° S	40.6772° S	40.6664° S
Longitude	148.078° E	148.226° E	148.092° E
Currents			
Sampling interval	-	150 s	60 s
Averaging interval	-	300 s	300 s
Number of samples	-	210	180
Blanking distance	-	0.5 m	0.4 m
Cell size	-	1 m	1 m
Measurement length	-	108 days	85 days
Standard deviation [1]	-	H: 1 cm/sB: 0.6 cm/s	H: 2.2 cm/sV: 0.7 cm/s
Turbulence			
Burst length	900 s	1200 s	-
Measurement interval	1800 s	3600 s	-
Sampling frequency	8 Hz	4 Hz	-
Beams	4 slanted	Vertical only	-
Blanking distance	0.1 m	0.5 m	-
Cell size	0.5 m	1 m	-
Measurement length	108 days	108 days	-
Standard deviation [1]	H: 3.44 cm/s B: 2.05 cm/s	V: 4.6 cm/s	-
Waves			
Sampling interval	-	2048 s	2048 s
Measurement interval	-	3600 s	3600 s
Sampling frequency	-	1 Hz	1 Hz
Number of samples	-	2048	2048
Measurement length	-	108 days	55 days
Standard deviation [1]	-	H: 1.4 cm/s B: 0.84 cm/s	H: 2.2 cm/s V: 0.7 cm/s

[1] Note: H: horizontal; V: vertical; B: beam. Values obtained from instruments' manufacturer software.

2.2. Theory Background

A velocity signal can be decomposed in:

$$u = \overline{u} + u_t' \quad (1)$$

where u represents the total velocity, $\overline{u}$ represents the mean velocity, usually averaged over 5 to 10 min, and u_t' represents the total instantaneous velocity fluctuation from the mean. However, in the presence of waves, a component relative to the wave orbital motion must be added. Hence, the decomposition becomes:

$$u = \overline{u} + u' + \widetilde{u} \quad (2)$$

where u' is the turbulent parcel of the velocity fluctuation and $\widetilde{u}$ is the orbital velocity. For a proper characterization of turbulence, the latter must be removed from the signal (2).

Estimation of turbulence parameters from data measured by an ADCP cannot be obtained directly from horizontal and vertical velocities [26]. Because of the geometry of the instrument and the beam spread, it is very likely that opposite beams will be sampling different turbulent eddies. However, the variance technique only relies on statistic features from each beam rather than the instantaneous values. This method requires two major assumptions: (a) spatial homogeneity between beams, which means the velocity fields sampled by opposite beams have the same statistical characteristics (mean velocity and velocity variance), and (b) turbulence is stationary over the averaging period [12,26]. The homogeneity assumption can be checked by estimating the velocity error E, defined as the difference between the two independent vertical velocities, which can be calculated by the two pairs of opposing beams. If the flow field is homogeneous, mean E is expected to be zero and this test is done by comparing E mean to its standard deviation. In a horizontally homogeneous flow, the mean should rarely exceed the standard deviation [12,36]. Therefore, wave-turbulence decomposition must be performed to beam velocities, prior to turbulence parameters estimation, rather than to streamwise, cross-stream, and vertical velocities directly.

TKE is a commonly used metric to characterize turbulence, which indicates the amount of energy contained in turbulent fluctuations per unit mass. It is traditionally defined as:

$$q^2 = \frac{\overline{u'^2} + \overline{v'^2} + \overline{w'^2}}{2} \tag{3}$$

where u', v', and w' indicate the turbulent velocity fluctuations in the streamwise, cross-stream, and vertical directions of the flow. The methodology for estimation of TKE from a 4-beams ADCP is fully described in the literature [12,26,27,37]. Because of the absence of true vertical measurements, an assumption regarding turbulence anisotropy is also necessary. This is done by adopting a value $\xi = \frac{\overline{w'^2}}{2}\frac{1}{q^2}$. Togneri and Masters [12], who have performed a similar estimation in a tidal energy site, followed the work of Nezu and Nakagawa [38], adopting $\xi = 0.1684$. Total TKE can, thus, be estimated from a 4-beams ADCP from:

$$TKE = \frac{\sum \overline{b'^2}_i}{4sin^2\theta(1 - \xi(1 - 2\,cot^2\theta))} \tag{4}$$

where $\overline{b'^2}$ is the beam variance over the averaging period and θ is the inclination angle of each beam from the vertical axis. For the Nortek Signature, instruments used in this study, this is equal to 25°.

Another important parameter for tidal turbine developers is TI, defined as:

$$TI = \frac{\sqrt{\overline{u'^2}}}{\overline{u}} \tag{5}$$

representing the portion of total velocity which is attributed to turbulent fluctuations and often given in percentages. Since TI results are influenced by the mean velocity, it is common practice to present and analyze both parameters together. Moreover, elevated TI are expected to happen during low mean current velocities, as in slack tide conditions, which could potentially lead to a misinterpretation of results.

The integral length scale is the turbulence scale containing the most energetic eddies. It can be estimated from the analysis of a temporal autocorrelation of velocity fluctuations which can be described as:

$$\rho(\tau) = \frac{\overline{u'(t)u'(t+\tau)}}{\overline{u'^2}} \tag{6}$$

where τ is a time increment given in seconds. The integral time scale can then be obtained by integrating $\rho(\tau)$ until the first zero-crossing point. By assuming Taylor's frozen field hypothesis, the integral

length scale can be calculated by multiplying the integral time scale by the average velocity [11]. Here, this analysis is performed over 5-min periods. It is important to highlight that it is necessary to assume the flow is homogeneous over the plane at which the streamwise velocity is calculated to estimate integral length scales from an ADCP in the streamwise direction. The distance from a velocity bin to the vertical axis above the instrument is equal to $d = 2zsin(\theta)$, where z is the vertical distance above the instrument [39,40]. Therefore, eddies smaller than d cannot be accurately resolved.

The significant wave height is defined as the height obtained from the wave energy spectrum as:

$$H_S = 4\sqrt{M_o} \tag{7}$$

where M_o is the variance of the water surface elevation, which is approximately equal to the sum of all frequency components of the wave energy spectrum. Given the depth of the channel, it is reasonable, as a first order approximation, to assume linear wave theory for wavelength estimation, defined as:

$$L = \frac{gT_p{}^2}{2\pi} \tag{8}$$

where T_p is the peak wave period, corresponding to the peak frequency for the wave spectrum.

2.3. Wave-Turbulence Decomposition Methods

2.3.1. Method 1: SB

The method described here uses a SB filter to remove the frequency bands in which waves are dominant in the velocity signal. To do so, an observation of the original energy spectrum is necessary in order to properly select the correct frequencies to be filtered. Data collected in Banks Strait indicated frequencies between 0.09 Hz and 0.16 Hz included orbital velocities. Hence these frequencies were selected as minimum and maximum thresholds in the second-order Butterworth filter which was applied to each beam velocity. This step was performed using the butter function in MATLAB (2018b, MathWorks, Natick, MA, USA). Even though recent works have pointed out the limitations of applying high-pass or bandpass filters in order to remove wave interference from the velocity signal, this method has successfully been applied in many studies, providing good estimates of TI [15,17,22]. In addition, this technique presents the benefit of requiring little computational resources.

2.3.2. Method 2: MA

The MA filter method is a technique that has been adopted by Williams et al. [28]. A simple MA filter is applied to the velocity signal in order to remove high frequency fluctuations. Therefore, the resulting signal is the portion of the signal composed strictly by low frequency fluctuations, which are assumed to be the wave orbital velocities. To perform the decomposition, the orbital velocities are subtracted from the original signal. The use of previous values in the moving average filter induces a slight time shift between the original and filtered signal. Therefore, to ensure the average is central to the data points, here the moving average filter is adapted to a two-sided moving average, defined as:

$$B_t = \frac{1}{2N+1}\sum_{i=-N}^{N} b_{t+i} \tag{9}$$

where B_t is the forecast value at instant t, N is the amount of values before and after the centre value to be averaged over and b_t is the value in the original signal at instant t. The filter is applied in order to obtain averaged values over a time period. A sensitivity analysis using periods of 1, 2, and 3 s was performed in order to identify the best time interval to be used. This indicated using 1 s provided the best result, reinforcing the choice made by Williams et al. [28]. The resulting filtered signal is expected to be approximate to the wave-induced motion and should then be subtracted from the original signal.

2.3.3. Method 3: SWT

The SWT is a time-frequency signal analysis method that has proved to be useful in extracting independent components from nonlinear and nonstationary signals. It uses a combination of a wavelet analysis and the reallocation method, reducing the energy spread and resulting in a more concentrated time-frequency analysis, which allows for the extraction of instantaneous frequencies [29]. This processing method has been applied for the first time with the purpose of decomposing wave and turbulence and described in detail by Bian et al. [21]. Here we have used a Morlet wavelet as performed by Daubechies et al. [29]. Daubechies et al. [29] and Thakur et al. [41] have shown the SWT is highly invariant to the mother wavelet shape and more affected to its concentration in time and frequency. Some other parameters that can be adjusted during the analysis are the number of voices per octave (recommendation is 32 or 64) and the number of curves to be extracted from the original signal. A more detailed description of the adjustable parameters can be found in Thakur et al. [41].

Initially, the original signal is decomposed in beam velocity mean and fluctuation. The SWT of the velocity fluctuation is then calculated in order to obtain the instantaneous frequencies of the signal. Wave dominant frequencies can then be identified as the most energetic frequencies and orbital velocity can be estimated by reconstructing the velocity fluctuation signal and summing it at the wave-dominant frequencies. To estimate turbulent fluctuations, the new reconstructed orbital velocity time-series is subtracted from the total velocity fluctuations. The MATLAB functions used to perform the described steps are part of the Synchrosqueezing Toolbox developed and made publicly available by Thakur et al. [41].

3. Results

3.1. Wave Climate Characterization

Table 2 shows the statistical results obtained from the analysis of the significant wave height and the period of the waves corresponding to the peak frequency for the wave spectrum. Analysis of wave data from instruments CWTb1 and CW4 indicates a considerable variation in significant wave height during the deployment period, with values ranging from approximately 0.5 m to over 5 m. Mean significant wave height observed in measurement locations CWTb1 and CW4 are 1.75 m and 1.42 m respectively, with approximately 75% of results below 2 m. Measured peak periods reveal dominance of long waves in Bank Straits, with maximum periods varying between 13 s and 15 s and mean values 8.05 s and 8.76 s at CWTb1 and CW4 respectively.

Table 2. Summary of statistical results of significant wave height and peak wave period from measurement locations CWTb1 and CW4. 1296 data points were included in the analysis for CWTb1 and 1342 data points for CW4.

	Statistical Variable	CWTb1	CW4
H_{Mo} (m)	Mean	1.75	1.42
	Standard deviation	0.78	1.03
	Maximum	5.17	5.26
	Minimum	0.49	0.04
	50th percentile	1.62	1.05
	75th percentile	2.25	2.01
T_P (s)	Mean	8.05	8.76
	Standard deviation	1.75	2.49
	Maximum	13.28	15.80
	Minimum	2.63	5.20
	50th percentile	7.97	7.79
	75th percentile	9.20	10.52

Figure 2 shows the significant wave height, peak wave period, and estimated wavelength time-series for the full deployment period. Results for 50th and 75th percentiles are illustrated by red and blue lines, with dashed lines corresponding to instrument CWTb1 and dotted lines to instrument CW4. Time-series agree well for both locations during the deployment, which indicates that waves exhibit similar characteristics across the entire channel in Banks Strait.

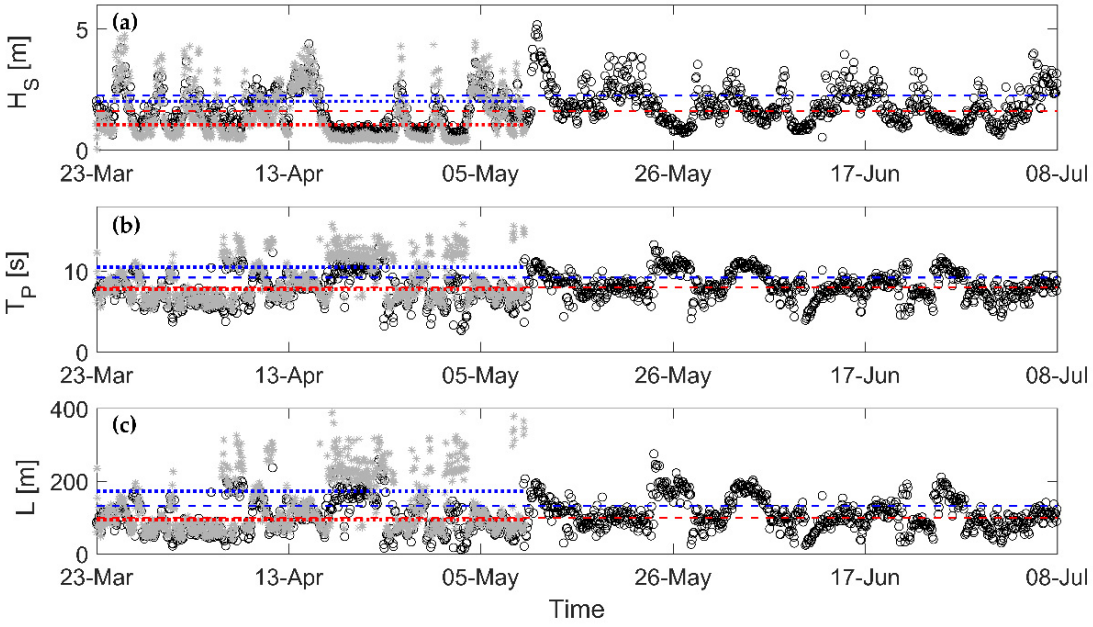

Figure 2. Time-series for (**a**) significant wave height, (**b**) peak wave period, and (**c**) estimated wavelength. Red and blue lines indicate 50th and 75th percentiles respectively. Black circles and dashed lines correspond to instrument CWTb1 and grey stars and dotted lines, to instrument CW4.

In order to characterize for the dominant wave direction, sea surface variance directional wave spectral densities obtained during the full deployment period were averaged (Figure 3). Reported directions correspond to the direction waves are coming from and peak direction occurrence is also presented in percentages in Table 3. The peak direction is related to the peak period obtained from the spectra. At both locations, waves come predominantly from West-Northwest (270°–315°) and East-Southeast (90°–135°) but at the measurement location CWTb1, waves exhibit a higher directional change.

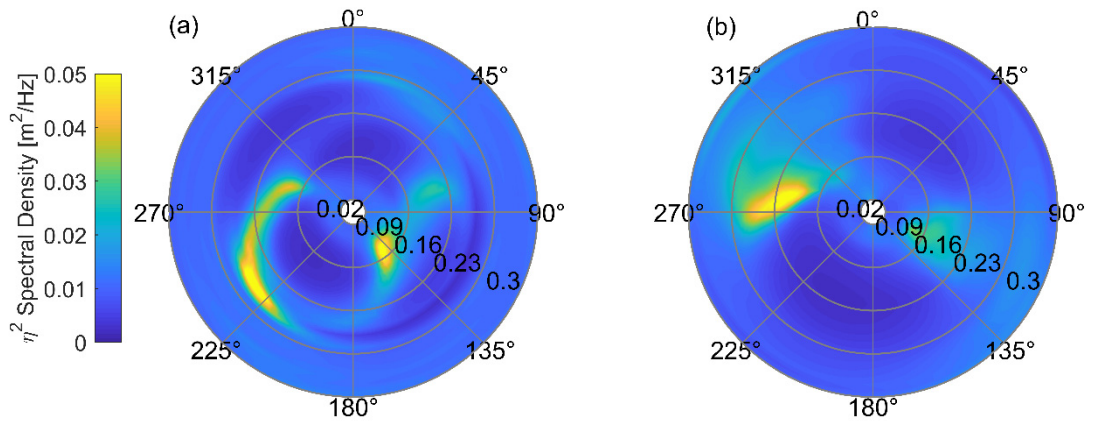

Figure 3. Averaged sea surface variance directional spectral density from instruments (**a**) CWTb1 and (**b**) CW4.

Table 3. Occurrence of peak wave direction from each station. Occurrence is presented in percentages and directions represent the direction the waves are coming from.

Peak Direction	CWTb1	CW4
0 < Dir ≤ 45°	1.00	2.83
45° < Dir ≤ 90°	10.65	6.33
90° < Dir ≤ 135°	22.92	33.08
135° < Dir ≤ 180°	16.28	0.60
180° < Dir ≤ 225°	3.63	0.07
225° < Dir ≤ 270°	8.80	0.22
270° < Dir ≤ 315°	35.65	52.16
315° < Dir ≤ 360°	1.08	4.69

3.2. Current Velocity Characterization

Table 4 summarizes the statistic results for current speeds measured with instruments CWTb1 and CW4. The 30% lowest values were removed from the data set so that slack tide would not be included. Current speeds have reached a maximum of 1.86 m/s and 2.35 m/s during ebb tide at locations CWTb1 and CW4 respectively. During flood tide, maximum currents reached 1.42 m/s and 2.23 m/s. Mean velocities were 0.85 m/s and 1.21 m/s during ebb tides and 0.67 m/s and 1.21 m/s during flood, indicating stronger currents during ebb tides at location CWTb1. Speed asymmetry here is defined as $|Ebb_{mean}/Flood_{mean}|$ to better understand the differences in current speeds during the two different stages of the tidal cycle.

Table 4. Summary of statistic results of current speed measured with instruments CWTb1 and CW4.

Statistic Result		CWTb-1		CW-4	
		Ebb	Flood	Ebb	Flood
Maximum speed	(m/s)	1.86	1.42	2.35	2.23
Mean speed		0.85	0.67	1.21	1.21
Standard deviation		0.28	0.17	0.31	0.30
Speed asymmetry	-	1.26		1.00	
Mean direction	(°)	117.13	280.91	104.79	292.16
Directional asymmetry		16.22		7.37	
Standard deviation		12.75	19.95	15.25	11.97

During ebb tides currents flowed dominantly to approximately 117.13° and 104.79° degrees from North, while during floods, these values are 280.91° and 292.16°, at locations CWTb1 and CW4 respectively. Figure 4 presents the current speed and direction for both stations and shows that current direction agrees well with the dominant wave direction. Asymmetry is defined as $|\overline{\theta}_{ebb} - \overline{\theta}_{flood} - 180°|$. Higher directional asymmetry—approximately 16.22°—is observed from data measured with instrument CWTb1, which was located in the Eastern part of the channel. Location CW4 presents a directional asymmetry of 7.37°.

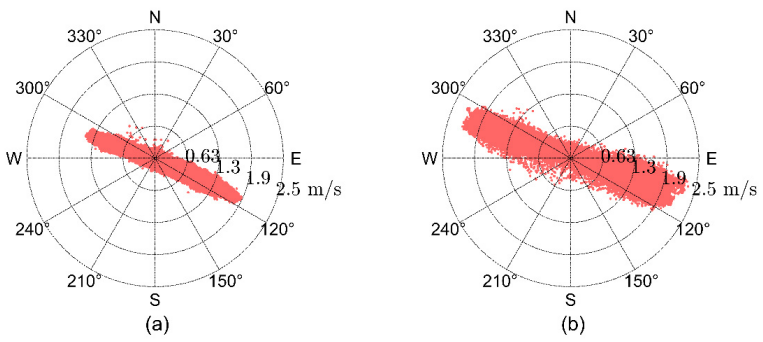

Figure 4. Current speed and direction from instruments (**a**) CWTb1 and (**b**) CW4.

3.3. Wave-Turbulence Decomposition Methods

3.3.1. Southern Part of the Channel

The original turbulent kinetic energy spectrum from a single 15-min burst measured with instrument CTb3 is shown in Figure 5. The burst was measured during fully developed spring flood tide, beginning at 6:30 PM on the 26th April 2018, when mean streamwise velocity was 1.26 m/s. A clear peak occurs at approximately 0.13 Hz. This frequency is consistent with wave peak frequencies measured at CW4. The peak is followed by the onset of the −5/3 slope, indicating that waves likely occur on the same frequency as larger turbulent eddies.

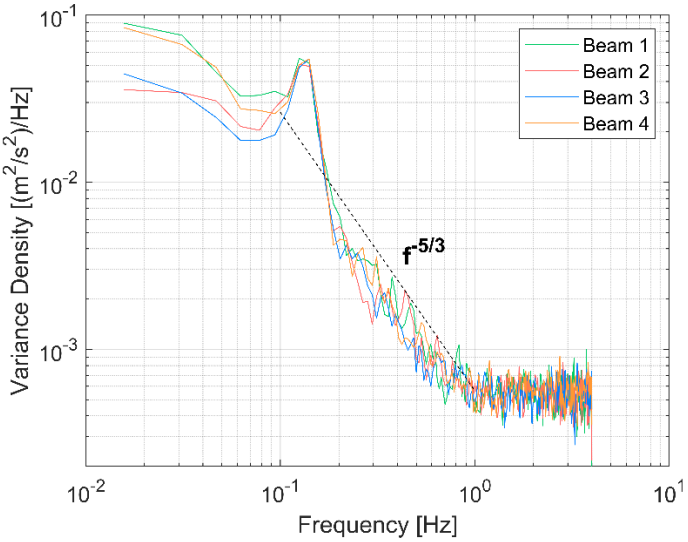

Figure 5. Original turbulent kinetic energy spectrum from velocities measured with each beam of instrument CTb3.

Results from wave-turbulence decomposition with the SB, MA, and SWT methods are shown in Figure 6. The column on the left-hand side of the figure shows a velocity time-series from beam 2 of the first 40 s of the same burst shown in Figure 5. A short period of the burst was selected to better visualize the low frequency orbital motion (Figure 6a,c,e). The right-hand side column shows the resulting turbulent kinetic energy spectrum of the burst. The time-series show the original velocity fluctuation, which is a sum of orbital velocities and turbulence, the estimated orbital velocity and the turbulent fluctuations, obtained after the removal of orbital motion from the original signal.

Although an initial comparison of the original velocity fluctuation and the estimated orbital velocity time-series shows good agreement, the spectra obtained from each method highlight the difference between these techniques. The spectrum resulting from the SB filter method presents a pronounced drop in energy over the frequencies in which wave interference was previously dominant, which yields a consequent underestimation of turbulent energy (Figure 6b). Likewise, a considerable drop in energy is observed from the MA filter method in the spectrum shown in Figure 6d, in which the −5/3 slope has vanished. In addition, a peak at the wave dominant frequencies is still present, indicating that this method was not sufficient in fully removing the orbital velocities from the analyzed signal. Looking at the orbital velocity time-series originated from this method (Figure 6 c), high frequency fluctuations are still visible, which justifies the significant decrease in turbulence. Finally, the application of the SWT method resulted in a slight drop in energy at the wave dominant frequencies, which can be observed in all beams but is more pronounced in beam 4 (Figure 6f). Generally, the resulting spectrum is in good agreement with the theoretical −5/3 slope, indicating less accentuated underestimation of turbulence. Moreover, orbital velocity time-series agrees well with the low frequency motion present in the original signal, suggesting a satisfactory performance.

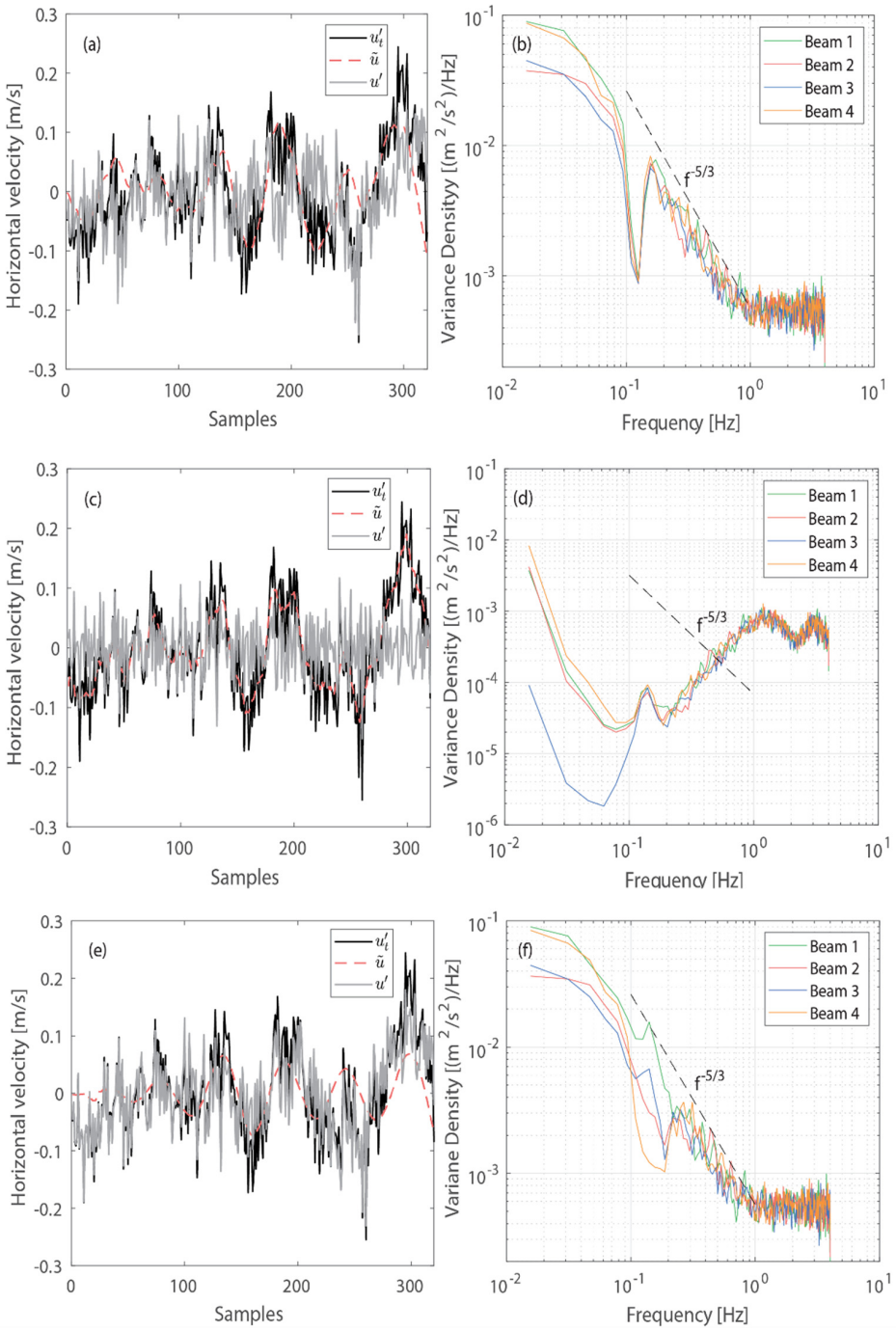

Figure 6. Original and decomposed velocity fluctuations time series from beam 2 and turbulent kinetic energy spectrum and after wave-turbulence decomposition performed in beam coordinates with (**a**,**b**) the stopband (SB) method, (**c**,**d**) moving average (MA) method, and (**e**,**f**) synchrosqueezing wavelet transform (SWT) method. Velocity time series obtained from beams 1, 3, and 4 presented similar results as beam 2. Mean streamwise velocity during this burst measurement was 1.26 m/s.

The performance of the three methods is also compared in Table 5, which shows averaged streamwise turbulence intensity and total TKE obtained from the same burst depicted in Figure 6. As expected from the analysis of the energy spectra, both turbulence intensity and TKE values are significantly underestimated by the MA method. While the SB and the SWT methods presented average turbulence intensities of approximately 11.50%, the MA method resulted in 6.02%. Similarly, average total TKE from this method is equal to nearly one-third of the result obtained from the other

two methods. In contrast to the spectral densities, the SB and the SWT decomposition methods reveal similar turbulence intensities (difference of 0.27%) and TKE (difference of 0.0001 m^2/s^2).

Table 5. Average turbulence intensity and total turbulent kinetic energy (TKE) from a 15-min long burst collected on the 26th April 2018 resulting from different wave-turbulence decomposition methods.

Method	Mean Streamwise TI (%)	Mean TKE (m^2/s^2)
SB	11.62	0.0162
MA	6.02	0.0048
SWT	11.35	0.0161

A period of approximately 12 h during spring tide on the 26th April 2018 was selected for the estimation of turbulence intensities and TKE in a complete tidal cycle using the three decomposition methods. Figure 7 shows turbulence intensity and velocity for the three depths at measurement location CTb3, estimated using each method. Results obtained from the SB filter and SWT methods do not differ significantly. Nonetheless, the MA method presents results considerably lower, reaching nearly half of TI and 1/4 of TKE obtained with the other methods. Generally, all methods reveal streamwise turbulence intensities that do not vary considerably between bottom tip, hub, and top tip heights.

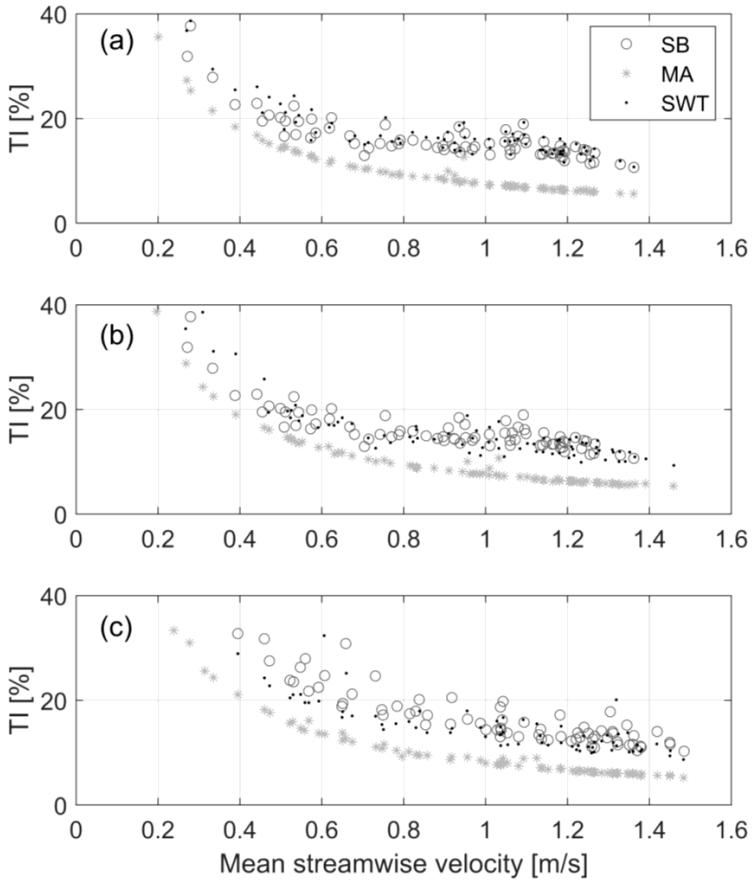

Figure 7. Streamwise turbulence intensities and mean velocity obtained with each method at (**a**) bottom tip height (10 m above seabed), (**b**) hub-height (15 m above seabed), and (**c**) top tip (20 m above seabed) from instrument CTb3.

The total TKE was also estimated at each depth using the three different decomposition methods. The resulting time-series for the full 12-h period is shown in Figure 8. As previously, the time-series obtained from the MA method significantly underestimates TKE, with values being approximately

four times smaller than the results obtained with the other two methods. Differences between bottom tip, hub height, and top tip are more prominent in the results from the SB method, with TKE slightly higher nearer the surface (top tip, in Figure 6a). Results originated from the SWT method do not seem to vary significantly between the three selected depths. Similarly to turbulence intensities estimates, total TKE obtained with the SB and the SWT methods do not differ substantially. Linear regression fit between TKE at hub-height from the two methods indicate highly similar results, with a regression coefficient of over 0.92 and R^2 of approximately 0.87 (Figure 9).

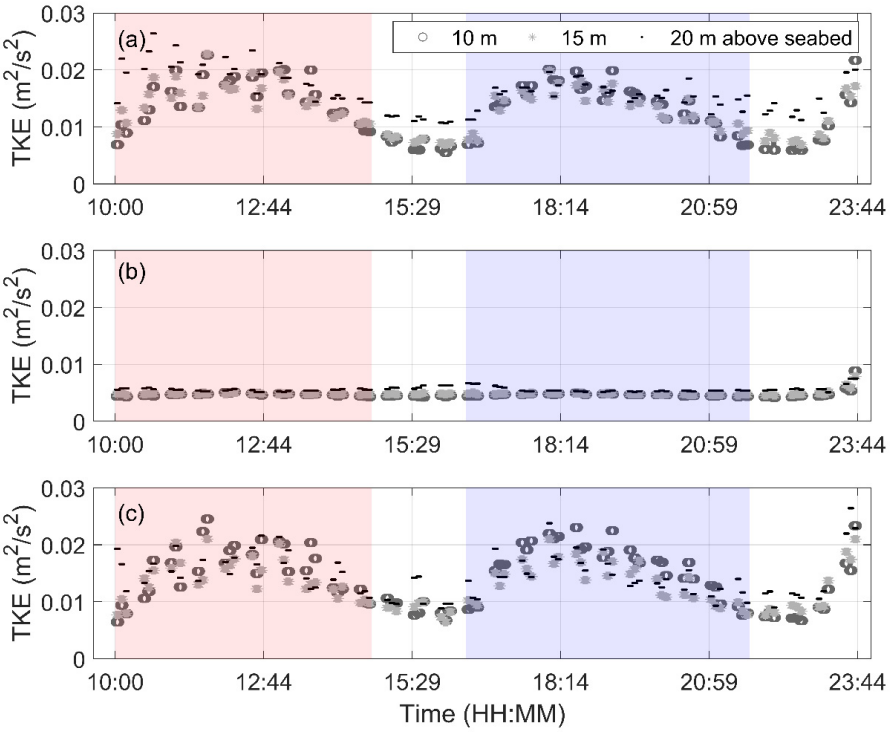

Figure 8. Total TKE estimated from (**a**) the SB, (**b**) MA, and (**c**) SWT decomposition methods at bottom tip height (10 m above seabed), hub-height (15 m above seabed), and top tip (20 m above seabed). Time-series show an approximately 12-h period, measured on the 26th April 2018 at measurement location CTb3. Red area shows ebb tide and blue area shows flood tide.

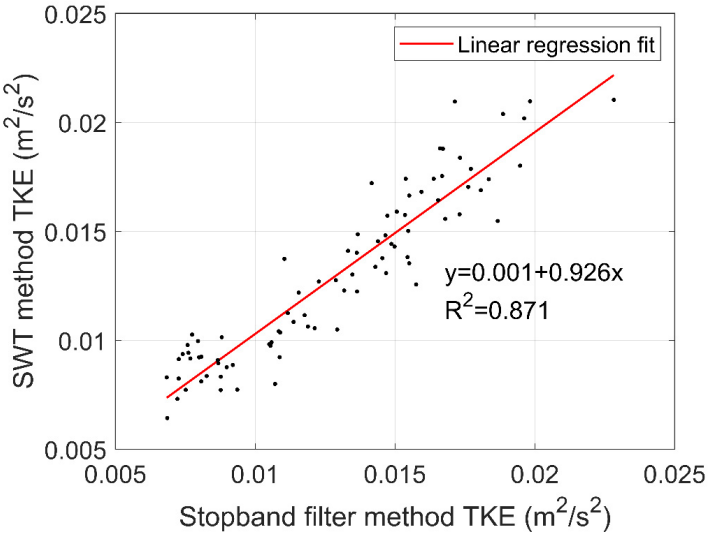

Figure 9. Linear regression fit between total TKE estimates at hub-height from instrument CTb3 obtained with the SB filter and the SWT methods.

3.3.2. Deep Pocket in the Center of the Channel

Because of the vertical beam measurements taken with the Signature 500 kHz (CWTb1), vertical TKE based on true vertical velocities could be estimated. Time-series of nearly the same times shown in Figure 8 are plotted in Figure 10. It is evident that values obtained after applying the SB and the SWT methods agree well, while results from the MA seem to considerably underestimate the TKE quantities. Linear regression fit for vertical TKE at hub-height demonstrates that the two methods perform similarly well (Figure 11).

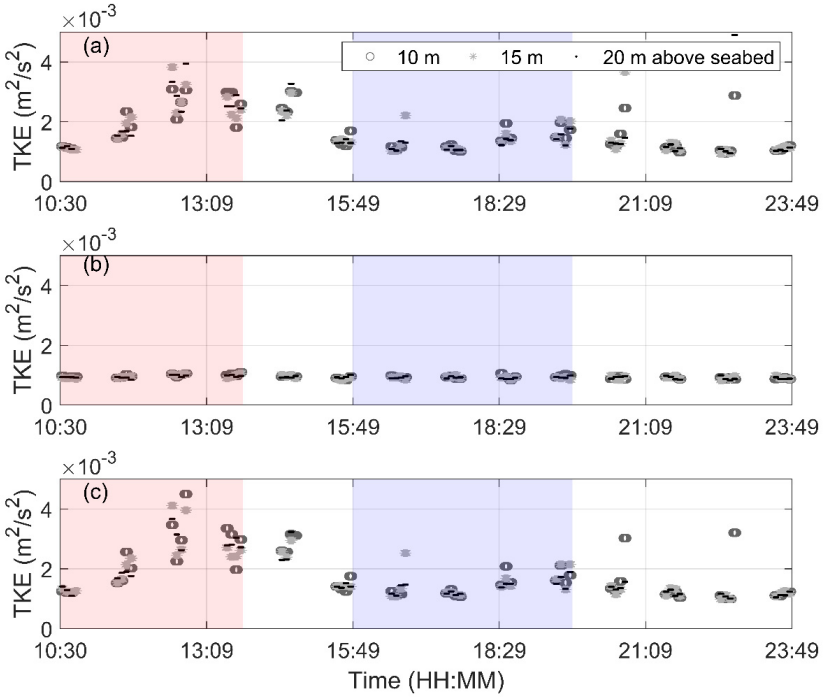

Figure 10. Vertical TKE estimated from vertical beam measurements using (**a**) the SB, (**b**) MA, and (**c**) SWT decomposition methods at bottom tip height (10 m above seabed), hub-height (15 m above seabed), and top tip (20 m above seabed). Time-series show an approximately 12-h period measured on the 26th April 2018 at measurement location CWTb1.

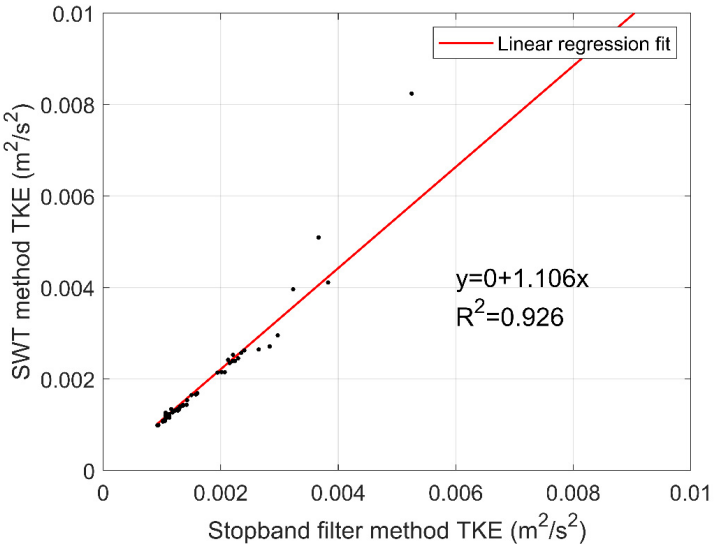

Figure 11. Linear regression fit between vertical TKE estimates at hub-height from instrument CWTb1 obtained with the SB filter and the SWT methods.

3.3.3. Integral Scales

Streamwise mean and maximum integral time and length scales from CTb3 for ebb and flood tides were also estimated for the two most successful methods (SB and SWT) (Table 6). Unlike TI and TKE estimates, results reveal a larger difference. For instance, for the top blade tip depth (20 m above the seabed) during ebb tides, mean integral length scale after the application of the SB was 2.13 m, while the value obtained from the SWT decomposed signal was 4.95 m. Generally, larger integral length scales are observed during ebb tide.

Table 6. Integral time and length scales from CTb3 estimated for ebb and flood tides based on streamwise velocity fluctuations obtained after the SB and the SWT methods.

Height		Tide	Integral Time Scale (s)		Integral Length Scale (m)	
			Mean	Max	Mean	Max
Bottom tip	SB	Ebb	9.12	24.57	9.56	26.91
		Flood	5.76	15.63	5.82	20.79
	SWT	Ebb	8.96	22.23	9.30	25.49
		Flood	4.89	14.35	4.97	19.07
Hub Height	SB	Ebb	5.67	20.41	6.56	25.93
		Flood	4.50	10.81	4.73	12.33
	SWT	Ebb	7.09	22.68	8.21	28.82
		Flood	4.79	14.74	4.87	12.25
Top tip	SB	Ebb	1.77	11.22	2.13	13.25
		Flood	2.75	9.21	3.09	9.78
	SWT	Ebb	4.08	17.51	4.95	20.74
		Flood	4.08	12.41	4.42	12.85

4. Discussion

Our data provide an overview of different techniques to decompose wave-current interaction during turbulent flow conditions in Banks Strait which is a candidate site for commercial development. Wave directions agree well with current direction, mostly at site CW4, as can be seen in Figures 3 and 4. Wave data collected with the Signature 500 kHz at CWTb1 indicate a higher directional spread. However, turbulent energy spectra from both sites reveal a pronounced peak at frequencies ranging from 0.1 Hz to 0.14 Hz, consistent with wave periods observed at both CWTb1 and CW4. This supports our findings of strong wave-current interaction at the sites, which is further corroborated by observations of low frequency fluctuations in the beam velocities.

Initial observation of the resulting turbulent energy spectra obtained after performance of wave-turbulence decomposition with the three tested methods indicates that the SWT method was the most successful. It induces a drop in energy at the wave-dominant frequencies, but this drop is not as accentuated when compared to the spectrum obtained with the SB method and agrees well with the expected −5/3 slope (Figure 6). Bian et al. [21] obtained similar results with an energy peak occurring at approximately 0.1 Hz, which is comparable to the peak frequency observed in Banks Strait. Variations in peak wave frequency could justify the poor performance of the MA method. This simple decomposition method has been introduced by Williams et al. [28] and successfully reproduced by Zhu et al. [18] but in both studies peaks occurred at higher frequencies in the spectrum (approximately 0.3 Hz). We hypothesize that this method reveals to be more suitable for higher frequency surface waves, which restricts its application for tidal energy sites exhibiting longer wave periods such as Banks Strait. The SWT was initially introduced by Daubechies et al. [29] and has been successfully applied to various fields of research over different frequency ranges (e.g., [29,41]). Nonetheless, this technique has never been tested in a tidal energy site and our findings show that this method present satisfactory results when performed to decompose wave and turbulence. More importantly, because of its proven versatility over a large wave frequency range it can be concluded that the SWT

method is also applicable at other tidal energy sites, which might have different wave-dominant frequencies compared to the data set presented here. Despite its robust and satisfactory performance, the SWT is also computationally expensive and, hence, time consuming, especially for analysis of large data sets from long deployments. For instance, the decomposition of a 12-h period of an AD2CP dataset with a sampling rate of 8 Hz took over 16 times the time required by the SB and the MA in the same computer. Therefore, applying this method to large data sets for long-term characterization and evaluation of seasonality is not trivial. In contrast, the SB method is computationally simple and easily replicable. The comparison between the SWT and SB methods has given satisfactory results in TI and TKE estimates. Interestingly, the application of this method for wave-turbulence decomposition has not considerably underestimated these turbulence parameters, when compared to the results obtained from the SWT method. Despite the difference in R^2 values obtained from the linear regression fit of TKE shown in Figures 9 and 11 (0.871 and 0.926 respectively) both have provided reasonable results. The slightly lower value obtained from total TKE from CTb3 is likely attributed to the fact that estimation of total TKE required the decomposition of the four beam velocity time-series, while vertical TKE estimation from CWTb1 only required the decomposition of a single velocity time-series. Since each beam velocity is decomposed separately, it is expected that four beams will yield a higher difference in TKE results versus a single beam. Both methods have provided turbulence intensities that are expected at tidal sites (10–15%) [10,42]. However, to ensure minimal turbulence underestimation when conducting the analysis to a long period, the SB method requires good knowledge of the wave dominant frequencies.

Integral length scales have been used to discuss tidal turbine performance (e.g., [4,8]) and poor estimation of this quantity represents a considerable disadvantage for tidal site assessments. Estimates of streamwise integral time and length scales obtained from the SB and SWT methods seem to yield a larger difference than that obtained for TI and TKE. With the exception of results produced during flood tides at bottom blade tip depth, the SB method produced smaller values, which led to the underestimation of turbulence. This difference becomes even more significant closer to the surface, and is likely attributed to the increase in distance between the bins of opposing beams. Estimation of integral length scales from ADCP measurements in the stream-wise direction can only be done by assuming flow homogeneity. In addition, the presence of eddies, which are larger than the water depth, demonstrates inherent anisotropy, since isotropic eddies are limited by the site depth [8]. Since the energy spectrum presents the peak right before the isotropic "−5/3" slope, waves are likely on the same frequency as these identified anisotropic large eddies. Our results suggest that the SB method should be used with caution while the SWT method is able to provide the tidal energy community more accurate estimates of integral scales. These findings also reinforce the results of other studies that the estimation of turbulence parameters can be biased by the presence of surface waves. For instance, Thiébaut et al. [43] has estimated turbulence dissipation rates and integral scales using ADCP data from Alderney Race, France. Their findings reveal estimated parameters were sensitive to wave-induced motion.

It is significant to highlight that the comparison between the wave-turbulence decomposition methods was performed in two measurement locations which present considerably different characteristics. While CTb3 is located in a 30-m deep area and presents strong current speeds, CWTb1 is located in a deep pocket in the center of the channel, being 60 m deep and presenting lower current speeds. This reveals that the presented results are valid under varying conditions.

5. Conclusions

The main goal of the present work was to test the decomposition methods for wave-turbulence interaction to provide turbine developers with information regarding blade loads for device design, ensuring long-term turbine integrity and facilitating tidal stream energy generation. In utilizing data collected from two Nortek Signature AD2CPs and a Nortek AWAC, wave and current characteristics were described and three wave-turbulence decomposition methods—the SB, the MA, and the SWT

methods—were compared. While the first two techniques are well-known and easily reproduceable, the third is a more complex and detailed signal processing tool. Mean wave periods were found to be nearly 8 s, but maximum wave periods exceeding 15 s extend the wave period spectrum significantly. Wave direction has shown to agree well with the current direction, reinforcing the previous findings of wave-current interaction at the site [32]. Findings reveal that poor choice of a wave-turbulence decomposition method likely leads to underestimation of fatigue loads, considerably putting long-term turbine integrity at risk.

Based on the estimated energy spectra, the MA method has highly underestimated the turbulence when compared to the other two methods. Streamwise turbulence intensities, turbulent kinetic energy, and streamwise integral time and length scales were estimated from the two most successful methods. Comparison between TI and TKE obtained after conducting the SB method has shown good agreement with those obtained with the SWT. A linear regression between total TKE at hub-height estimated from instrument CTb3 from the two methods indicated similar results. The same analysis was done for vertical TKE estimated from instrument CWTb1. Nonetheless, estimates of streamwise integral scales from the SB and the SWT methods have resulted in a larger difference, especially for the top blade tip depth. Since variations in turbulence length scales have been shown to affect the tidal turbines performance, the consequent underestimation of this parameters from the SB filter method represents a considerable disadvantage when performing a tidal energy site assessment. These diverging turbulence estimates obtained from different methods highlight the need to implement assessment guidelines which address the issue of wave-turbulence interaction at tidal energy sites.

The data collected in Banks Strait help advancing the knowledge about suitable decomposition techniques, but further investigation is necessary to assess the performance of these decomposition methods at sites that are home to different wave climates. Despite being computationally expensive and highly time consuming the SWT has also shown to provide the most accurate estimates of turbulence parameters, facilitating improved quantification of estimated fatigue loads and as such advancing the design and longevity of tidal turbine devices.

Supplementary Materials: The datasets used in this research are publicly available at: https://doi.org/10.14264/ab5f3c0.

Author Contributions: L.P. worked on the conceptualization of this paper, its methodology, data processing and analysis, as well as writing the original draft. R.C. and I.P. have substantially contributed to this paper through funding acquisition, project administration, data collection, improvements on data analysis, as well as supervising and reviewing. C.C. has added to this work through data collection and processing. All authors have read and agreed to the published version of the manuscript.

Funding: The AUSTEn Project is co-funded by the Australian Renewable Agency (ARENA) through the Advancing Renewables Programme (grant G00902), the Australian Maritime College (University of Tasmania), the University of Queensland, CSIRO Oceans and Atmosphere, CSIRO Energy, our industry partners, SIMEC Atlantis Energy and MAKO Tidal Turbines.

Acknowledgments: The authors would like to thank Professor Alex Hay from Dalhousie University, Canada.

Conflicts of Interest: The authors declare no conflict of interest.

Abbreviations

ADCP	Acoustic Doppler Current Profiler
AD2CP	New generation 5-beam Nortek ADCP
ADV	Acoustic Doppler Velocimeter
AUSTEn	Australian Tidal Energy Project
AWAC	Nortek Acoustic Wave and Current Profiler
LCOE	Levelized Cost of Energy
MA	Moving Average filter
SB	Stopband filter
SWT	Synchrosqueezing Wavelet Transform
TI	Turbulence Intensity

TKE	Turbulence Kinetic Energy
u	Total velocity
$\overline{u}$	Mean velocity
$u_t{}'$	Total velocity fluctuation
u'	Turbulent fluctuation
$\widetilde{u}$	Wave orbital velocity
q^2	Turbulent kinetic energy
b'_i	ith beam velocity fluctuation
θ	ADCP beam slanted angle
ξ	Constant for anisotropy assumption
ρ	Autocorrelation function
τ	Time increment in the autocorrelation function
H_S	Significant wave height estimated from wave spectrum
M_o	Variance in the water surface elevation
L	Wavelength
T_p	Peak wave period

References

1. Copping, A.; Battey, H.; Brown-Saracino, J.; Massaua, M.; Smith, C. An international assessment of the environmental effects of marine energy development. *Ocean Coast. Manag.* **2014**, *99*, 3–13. [CrossRef]
2. Harrold, M.; Ouro, P. Rotor Loading Characteristics of a Full-Scale Tidal Turbine. *Energies* **2019**, *12*, 1035. [CrossRef]
3. Milne, I.A.; Day, A.H.; Sharma, R.N.; Flay, R.G.J. The characterisation of the hydrodynamic loads on tidal turbines due to turbulence. *Renew. Sustain. Energy Rev.* **2016**, *56*, 851–864. [CrossRef]
4. Ouro, P.; Stoesser, T. Impact of Environmental Turbulence on the Performance and Loadings of a Tidal Stream Turbine. *Flow Turbul. Combust.* **2019**, *102*, 613–639. [CrossRef]
5. Vazquez, A.; Iglesias, G. A holistic method for selecting tidal stream energy hotspots under technical, economic and functional constraints. *Energy Convers. Manag.* **2016**, *117*, 420–430. [CrossRef]
6. Li, W.; Zhou, H.; Liu, H.; Lin, Y.; Xu, Q. Review on the blade design technologies of tidal current turbine. *Renew. Sustain. Energy Rev.* **2016**, *63*, 414–422. [CrossRef]
7. Lewis, M.; Mcnaughton, J.; Márquez-Dominguez, C.; Todeschini, G.; Togneri, M.; Masters, I.; Allmark, M.; Stallard, T.; Neill, S.; Goward-Brown, A.; et al. Power variability of tidal-stream energy and implications for electricity supply. *Energy* **2019**, *183*, 1061–1074. [CrossRef]
8. Blackmore, T.; Myers, L.E.; Bahaj, A.S. Effects of turbulence on tidal turbines: Implications to performance, blade loads, and condition monitoring. *Int. J. Mar. Energy* **2016**, *14*, 1–26. [CrossRef]
9. Mycek, P.; Gaurier, B.; Germain, G.; Pinon, G.; Rivoalen, E. Experimental study of the turbulence intensity effects on marine current turbines behaviour. Part I: One single turbine. *Renew. Energy* **2014**, *66*, 729–746. [CrossRef]
10. Thomson, J.; Polagye, B.; Durgesh, V.; Richmond, M.C. Measurements of Turbulence at Two Tidal Energy Sites in Puget Sound, WA. *IEEE J. Ocean. Eng.* **2012**, *37*, 363–374. [CrossRef]
11. McCaffrey, K.; Fox-Kemper, B.; Hamlington, P.E.; Thomson, J. Characterization of turbulence anisotropy, coherence, and intermittency at a prospective tidal energy site: Observational data analysis. *Renew. Energy* **2015**, *76*, 441–453. [CrossRef]
12. Togneri, M.; Masters, I. Micrositing variability and mean flow scaling for marine turbulence in Ramsey Sound. *J. Ocean. Eng. Sci.* **2016**, *2*, 35–46. [CrossRef]
13. Hay, A.E.; McMillan, J.; Cheel, R.; Schillinger, D. Turbulence and Drag in a High Reynolds Number Tidal Passage Targetted for In-Stream Tidal Power. In Proceedings of the 2013 OCEANS-San Diego, San Diego, CA, USA, 23–27 September 2013; pp. 1–10.
14. Guerra, M.; Thomson, J. Turbulence Measurements from Five-Beam Acoustic Doppler Current Profilers. *J. Atmos. Ocean. Technol.* **2017**, *34*, 1267–1284. [CrossRef]
15. Smyth, C.; Hay, A.E.; Zedel, L. Coherent Doppler Profiler measurements of near–bed suspended sediment fluxes and the influence of bed forms. *J. Geophys. Res. Oceans* **2002**, *107*, 19-1–19-20. [CrossRef]

16. Filipot, J.-F.; Prevosto, M.; Maisondieu, C.; Le Boulluec, M.; Thomson, J. Wave and turbulence measurements at a tidal energy site. In Proceedings of the 2015 IEEE/OES Eleventh Current, Waves and Turbulence Measurement (CWTM), St Petersburg, FL, USA, 2–6 March 2015; pp. 1–9.
17. Newgard, J.P.; Hay, A.E. Turbulence intensity in the wave boundary layer and bottom friction under (mainly) flat bed conditions. *J. Geophys. Res. Oceans* **2007**, *112*. [CrossRef]
18. Zhu, Q.; van Prooijen, B.C.; Wang, Z.B.; Ma, Y.X.; Yang, S.L. Bed shear stress estimation on an open intertidal flat using in situ measurements. *Estuar. Coast. Shelf Sci.* **2016**, *182*, 190–201. [CrossRef]
19. Parkinson, S.G.; Collier, W.J. Model validation of hydrodynamic loads and performance of a full-scale tidal turbine using Tidal Bladed. *Int. J. Mar. Energy* **2016**, *16*, 279–297. [CrossRef]
20. Bricker, J.D.; Monismith, S.G. Spectral wave-turbulence decomposition. *J. Atmos. Ocean. Technol.* **2007**, *24*, 1479–1487. [CrossRef]
21. Bian, C.; Liu, Z.; Huang, Y.; Zhao, L.; Jiang, W. On Estimating Turbulent Reynolds Stress in Wavy Aquatic Environment. *J. Geophys. Res. Oceans* **2018**, *123*, 3060–3071. [CrossRef]
22. Foster, D. *Dynamics of the Nearshore Wave Bottom Boundary Layer*; ProQuest Dissertations Publishing: Washington, DC, USA, 1997.
23. Meirelles, S.; Henriquez, M.; Horner-Devine, A.R.; Souza, A.J.; Pietrzak, J.; Stive, M. Bed Shear Stress on the middle shoreface of the South-Holland Coast. In Proceedings of the Coastal Sediments 2015, San Diego, CA, USA, 11–15 May 2015.
24. Soulsby, R.L.; Humphrey, J.D. Field observations of wave-current interaction at the sea bed. In *Water and Wave Kinematics*; Springer: Dordrecht, The Netherlands, 1990; Volume 178, pp. 413–428.
25. Kolmogorov, A.N. The Local Structure of Turbulence in Incompressible Viscous Fluid for Very Large Reynolds' Numbers. *Dokl. Akad. Nauk* **1941**, *30*, 301–305. [CrossRef]
26. Stacey, M.; Monismith, S.; Burau, J. Measurements of Reynolds stress profiles in unstratified tidal flow. *J. Geophys. Res. Oceans* **1999**, *104*, 10933–10949. [CrossRef]
27. Lu, Y.; Lueck, R. Using a broadband ADCP in a tidal channel. Part II: Turbulence. *J. Atmos. Ocean. Technol.* **1999**, *16*, 1568–1579. [CrossRef]
28. Williams, J.J.; Bell, P.S.; Thorne, P.D. Field measurements of flow fields and sediment transport above mobile bed forms. *J. Geophys. Res. Oceans* **2003**, *108*. [CrossRef]
29. Daubechies, I.; Lu, J.; Wu, H.-T. Synchrosqueezed wavelet transforms: An empirical mode decomposition-like tool. *Appl. Comput. Harmonic Anal.* **2011**, *30*, 243–261. [CrossRef]
30. Penesis, I.; Hemer, M.; Cossu, R.; Hayward, J.; Nader, J.-R.; Rosebrock, U.; Grinham, A.; Sayeef, S.; Osman, P.; Marsh, P. Tidal energy in Australia—Assessing resource and feasibility to Australia's future energy mix. In Proceedings of the Asian Wave and Tidal Energy Conference, Taipei, Taiwan, 9–13 September 2018.
31. Marsh, P.; Penesis, I.; Nader, J.-R.; Couzi, C.; Cossu, R. Assessment of tidal current resources in Banks Strait, Australia. In Proceedings of the European Wave and Tidal Energy Conference, Naples, Italy, 1–6 September 2019.
32. Perez, L.; Cossu, R.; Penesis, I.; Grinham, A.; Nader, J.-R.; Couzi, C. A case study of high frequency AD2CP measurements for tidal site characterization in Banks Straits, Tasmania, Australia. In Proceedings of the European Wave and Tidal Energy Conference, Naples, Italy, 1–6 September 2019.
33. Rahimi, R.; Penesis, I.; Hemer, M.; Mason, L.; Thomas, G.J.R.E. Characterization of the tidal current resource in Tasmania. In Proceedings of the Asian Wave and Tidal Energy Conference, Tokyo, Japan, 28–30 July 2014.
34. Bureau of Meteorology (BOM). Climate data online—Swan Island (092123). Available online: http://www.bom.gov.au/climate/ (accessed on 20 April 2019).
35. Shcherbina, A.Y.; D'Asaro, E.A. Observing Finescale Oceanic Velocity Structure with an Autonomous Nortek Acoustic Doppler Current Profiler. *J. Atmos. Ocean. Technol.* **2018**, *35*, 411–427. [CrossRef]
36. Lu, Y.; Lueck, R.G. Using a broadband ADCP in a tidal channel. Part I: Mean flow and shear. *J. Atmos. Ocean. Technol.* **1999**, *16*, 1556–1567. [CrossRef]
37. Togneri, M.; Jones, D.; Neill, S.; Lewis, M.; Ward, S.; Piano, M.; Masters, I. Comparison of 4- and 5-beam acoustic Doppler current profiler configurations for measurement of turbulent kinetic energy. *Energy Procedia* **2017**, *125*, 260–267. [CrossRef]
38. Nezu, I.; Nakagawa, H. *Turbulence in Open-Channel Flows*; A. A. Balkema Publishers: Rotterdam, The Netherlands, 1993.

39. Greenwood, C.; Vogler, A.; Venugopal, V. On the Variation of Turbulence in a High-Velocity Tidal Channel. *Energies* **2019**, *12*, 672. [CrossRef]
40. Bouferrouk, A.; Hardwick, J.P.; Colucci, A.M.; Johanning, L. Quantifying turbulence from field measurements at a mixed low tidal energy site. *Renew. Energy* **2016**, *87*, 478–492. [CrossRef]
41. Thakur, G.; Brevdo, E.; Fučkar, N.S.; Wu, H.-T. The Synchrosqueezing algorithm for time-varying spectral analysis: Robustness properties and new paleoclimate applications. *Signal Process.* **2013**, *93*, 1079–1094. [CrossRef]
42. Milne, I.A.; Sharma, R.N.; Flay, R.G.J.; Bickerton, S. Characteristics of the turbulence in the flow at a tidal stream power site. *Philos. Trans. R. Soc. A* **2013**, *371*. [CrossRef] [PubMed]
43. Thiébaut, M.; Filipot, J.F.; Maisondieu, C.; Damblans, G.; Duarte, R.; Droniou, E.; Chaplain, N.; Guillou, S. A comprehensive assessment of turbulence at a tidal-stream energy site influenced by wind-generated ocean waves. *Energy* **2020**, *191*, 116550. [CrossRef]